Materials Today Bio 32 (2025) 101700

Contents lists available at ScienceDirect

Materials Today Bio

journal homepage: www.journals.elsevier.com/materials-today-bio

Engineering a dynamic extracellular matrix using thrombospondin-1 to propel hepatocyte organoids reprogramming and improve mouse liver regeneration post-transplantation

Zi-Yan Xu [a,1], Min Wang [a,1], Jing-Yan Shi [b,1], Ye Liu [c,1], Chao Yu [a], Xin-Yi Zhang [a], Chen-Wei Zhang [a], Qi-Feng He [a], Chao Pan [a], Jin Zhou [a], Hua Xiao [a,*], Hong-Yong Cao [a,**], Yong Ma [a,***]

[a] Department of General Surgery, Nanjing First Hospital, Nanjing Medical University, Nanjing, China
[b] Nanjing Drum Tower Hospital, The Affiliated Hospital of Nanjing University Medical School, Nanjing, China
[c] School of Medicine, Southeast University, Nanjing, China

ARTICLE INFO

Keywords:
Hepatocyte organoids (HOs)
Liver regeneration
Reprogramming
Extracellular matrix (ECM)
Thrombospondin-1 (THBS1)
Transplantation

ABSTRACT

Hepatocyte organoids (HOs) hold significant potential for constructing bioartificial liver construction, toxicology research, and liver failure therapies. However, challenges such as difficulties in induced pluripotent stem cells (iPSCs) harvest and differentiation, safety concerns of tumor-derived matrices, and limited primary cell regulation hinder clinical applications. In this study, we developed a non-tumor-derived decellularized extracellular matrix (dECM) system with tunable mechanical properties and viscoelasticity to enhance stem cell proliferation and organoid functionality using thrombospondin-1 (THBS1). Nanoindentation and transcriptomic analysis revealed that THBS1 mediates adaptation and remodeling between organoids and ECM proteins, exhibiting native tissue-like viscoelasticity and up-regulated reprogramming transcriptional factors KLF4 and SOX2 via the YAP/TAZ pathway. Transplanting HOs presenting reprogramming effects into a 70 % hepatectomy model demonstrated improved liver regeneration, underscoring the potential of the THBS1-based dynamic ECM system in organoids manipulation and liver regeneration.

1. Introduction

The liver performs indispensable physiological functions, including metabolism, synthesis, digestion, detoxification, and excretion [1]. Owing to the robust differentiation and proliferation potential of hepatic progenitor cells (HPCs), the liver exhibits a remarkable capacity for regenerative, allowing it to restore full functionality even after losing up to 70 % of its mass [2]. However, in cases of end-stage liver cancer, advanced cirrhosis, or congenital metabolic disorders, this regenerative capacity becomes insufficient, leading to liver failure. When the liver reaches a state of decompensation, its ability to sustain vital functions is severely compromised, ultimately resulting in death.

Liver transplantation is currently the most effective treatment for end-stage liver failure, however the severe global shortage of liver donors significantly limits its availability [3]. Organoid technology offers a promising alternative, as it enables the expansion of liver cells that can reliably propagate in vitro and differentiate into functional hepatocytes or biliary epithelial cells (BECs). These cells exhibit enhanced microenvironment homing efficiency and repair capacity, making them an ideal source for autologous stem cell transplantation and a critical component in artificial liver systems [4–6].

However, the indispensable role of Matrigel in organoid culture and the limited options for in vitro regulation of stem cells restrict the clinical application of HOs [5,7]. First, Matrigel exhibits batch-to-batch variations in protein content, particularly structural proteins, which compromise experimental consistency and reproducibility [8,9]. Additionally, growth factor levels vary significantly between batches, with proteomics analysis revealing only about 53 % similarity in factors

* Corresponding author.
** Corresponding author.
*** Corresponding author. Department of General Surgery, Nanjing First Hospital, Nanjing Medical University, Nanjing, China.
E-mail addresses: xiaohua0726_x@163.com (H. Xiao), caohongy6167@163.com (H.-Y. Cao), yma0917@163.com (Y. Ma).
[1] There authors have contributed equally to this work and share first authorship.

https://doi.org/10.1016/j.mtbio.2025.101700
Received 14 January 2025; Received in revised form 9 March 2025; Accepted 22 March 2025
Available online 25 March 2025

between batches of growth-factor-reduced (GFR) Matrigel. This variability has led many researchers to advocate for cautious interpretation of organoid studies based on Matrigel [10]. Second, the macromolecular laminin (LN) subtypes, one of the primary components of the cross-linked network, are diverse and unevenly concentrated, making chemical modification of Matrigel's cross-linking process challenging. Moreover, its insufficient mechanical strength further limits its suitability for various tissue organoid development, bioprinting, and scaffold construction. Third, Matrigel's tumor-derived origin and potential contamination from tumor tissues have raised safety concerns [11,12].

To address this challenge, we focused on decellularized extracellular matrix (dECM) as a popular alternative, which offers several advantages over other synthetic or natural materials. dECM retains the composition and structure specific to the cellular microenvironment, providing essential signals for cell homing, proliferation, and self-assembly in vitro, along with mechanical properties suitable for native tissue cell growth and organization. A few studies have confirmed the feasibility of using dECM hydrogels derived from human or porcine tissues for culturing organoids from corresponding tissues, such as the intestine, lungs, liver, and bladder [12–14]. In addition, a well-defined and adjustable culture environment was envisaged in combination with gelatin methacrylate (GelMA) rich in inherent Arg-Gly-Asp (RGD) sequences, which facilitate organoid encapsulation and budding. As a biosafe and bioactive modified gelatin product, GelMA provides a tunable environment, which is believed to play a critical role in controlling stem cell behavior and organoid growth [15,16]. However, how the interactions between ECM and stem cells can be leveraged to achieve controlled organoid differentiation and enhanced functionality in vitro remains insufficiently explored.

Recently, there has been a surge in reports on the impact of the mechanical properties of the extracellular matrix (ECM) on cancer cell progression and stem cell regulation [17,18]. To modulate ECM properties in our dECM system, we focused on Thrombospondin-1 (THBS1) as it has emerged as a key signaling bridge between cells and surrounding ECM proteins, which regulates the degradation and synthesis of ECM proteins in the cellular microenvironment through matrix metalloproteinase-9 (MMP-9) and focal adhesion kinase (FAK), thereby exhibiting viscoelastic behavior at the micromechanical level that is closely resembles native tissues and organs [19,20]. However, whether the mechanical signals generated by THBS1 can be sensed by stem cells to achieve dynamic regulation of organoid differentiation and maturation, as well as the specific interrelation between variation in hepatocyte transcriptional characteristics and post-transplantation repair capabilities, remains inadequately studied.

In this study, we investigated THBS1 as a novel modulator of viscoelasticity in a dECM system engineered with adjustable mechanical properties to achieve a more dynamic and controlled microenvironment for hepatic organoid development and functionality. Our objective was to explore the interactions between matrix microenvironment properties, organoid transcriptional expression, and post-transplantation cellular function. We found that THBS1 induces dynamic changes in dECM properties by activating MMPs and FAK, which drive hepatocyte reprogramming through Hippo-YAP signaling, thereby altering the differentiation patterns and cellular function of HOs. Inspired by the role of the Notch-YAP1/TEAD pathway in hepatocellular reprogramming, we conducted a canonical hepatocellular reprogramming experiment using retroviral vectors expressing Oct4, Sox2, Klf4, and c-Myc, which helped us delineate the changes driven by THBS1 in HOs. Notably that a significant proportion of hepatocytes in HOs underwent reprogramming effects following THBS1 treatment, a phenomenon akin to the reprogramming observed in the HOs transfected with Oct4, Sox2, Klf4, and c-Myc. These changes ultimately enhanced liver regeneration and improves liver function in a mouse model of hepatectomy-induced liver failure following organoid transplantation (OT).

2. Materials and methods

Decellularization procedure of porcine livers. Fresh liver tissue from male Landrace pigs (Jiangsu Hurun Agricultural Products Co. Ltd) was harvested and cut into pieces measuring 5 mm × 5 mm × 2 mm within 4 h after collection. The tissue slices were initially rinsed under pressurized water for 1 h, followed by gentle washing with distilled water for an additional hour, after which they were shaken overnight at 4 °C. For decellularization, the slices were immersed in specific detergents under the following conditions:

Ammonium Hydroxide dECM (AHdECM) group: 0.1 % (v/v) AH (Sigma, 05002) combined with 1 % Triton X-100 (Sigma, T8787), agitated at room temperature (RT) for 48 h.

Sodium Deoxycholate dECM (SDCdECM) group: 4 % SDC (Sigma, D6750) mixed with 1 % Triton X-100, agitated at RT for 4 h.

Sodium Dodecyl Sulfate dECM (SDSdECM) group: 1 % SDS (Sigma, 436143) combined with 1 % Triton X-100, agitated at RT for 48 h [12,21].

After decellularization, the slices were rinsed with distilled water at 4 °C with agitation for 24 h, with the water changed every 6 h. The samples were then treated with 2000 kU of DNase-I (Sigma, 10104159001) in 1M NaCl at RT for 3 h to digest residual DNA. Following this, the samples were rinsed again with distilled water at 4 °C for 48 h to remove residual enzymes, with the water changed every 4 h. Once rinsed, the samples were lyophilized and milled into a fine powder passing through a 100-μm mesh (Biosharp, BS-100-XBS). The dECM powder was then sterilized in a solution of 0.1 % peracetic acid (Acros, C25775) combined with 4 % ethanol for 4 h at 4 °C, followed by rinsing with distilled water. The resulting powder was lyophilized and stored at −20 °C [22].

2.1. Confirmation of decellularization

Histochemistry: Untreated or treated tissues were fixed in 4 % paraformaldehyde (PFA). After fixation, the samples underwent dehydration and paraffin embedding. The embedded samples were sectioned and subjected to various staining techniques, including hematoxylin and eosin (HE), Masson's trichrome stain, alcian blue-periodic acid-Schiff (AB-PAS), and diamidino-phenyl-indole (DAPI) staining.

DNA quantification: Samples were randomly collected before and after detergent treatment [12]. The DNA content was assessed using a PureLink Genomic DNA Mini Kit (Thermo Fisher, K182000) and quantified with a NanoDrop microvolume spectrophotometer (Thermo Fisher, ND-ONEC-W).

dECM contents. After digestion, samples were collected from the pre-gel, and the main components of the decellularized extracellular matrix (dECM) were quantified using a collagen enzyme-linked immunosorbent assay (ELISA) Kit (Thermo Fisher, MAK322), a laminin ELISA Kit (XIGE, E990261), and a glycosaminoglycan (GAG) ELISA Kit (BOKE, F99675). The final concentrations were determined using a spectrophotometer (Potenov, PT-3502PC) [12,23].

LC-MS/MS. Protein identification of the decellularized tissues was performed using liquid chromatography-tandem mass spectrometry (LC-MS/MS). Proteins were extracted from the tissues using a methanol-chloroform solution as previously described [24]. The samples were digested with trypsin (Thermo Fisher, 25200072) overnight at 37 °C, and the resulting peptides were labeled with isobaric tags for relative and absolute quantitation (iTRAQ) 8-plex. Each peptide fraction was dissolved in a solution of 5 % acetonitrile (HUSHI, 75-05-8) and 0.1 % formic acid (HUSHI, 64-18-6), followed by centrifugation at 20,000×*g* for 10 min. The supernatant was pre-separated using a Shimadzu LC-20AD Nano-HPLC system. Separated peptides were then analyzed using the AB SCIEX Triple TOF 5600 system (Concord). Data processing and protein identification were conducted using the WebGestalt toolkit. iTRAQ protein identification and quantification were performed using the Mascot 2.3.02 search engine (Matrix Science) [25]. Protein

abundance across different biological replicates was compared, and the ratio of each protein in each comparison was normalized to 1. Differences in protein abundance were represented as a percentage of the quantified proteins.

Hydrogel preparation. Stored dECM powder was digested in a pepsin/hydrochloric acid solution (P6887, Sigma-Aldrich) at a concentration of 1 mg/mL in 0.01 M hydrochloric acid, with varying concentrations of 6, 8, 10, and 12 mg/mL, at room temperature under constant magnetic stirring for 72 h [12,22]. Large particles were removed by centrifugation at 2000 rpm for 5 min. The resulting pre-gel was neutralized to a physiological pH of 7.4 using a 0.1 M NaOH solution. Gelation of the pre-gel was induced at 37 °C. To prepare the dECM-GelMA composite hydrogel, GelMA (5, 10, 15, or 20 mg/mL) (Sigma, 10104159001) and 0.1 % LAP (Aladdin, L157759) were added to the dECM pre-gel. The mixture was stirred continuously at 30 °C for 1 h to ensure complete dissolution of the components [26].

2.2. Mechanical characterization

Elastic modulus. The elastic modulus of the hydrogel was determined using compression testing. Cylindrical samples (5 mm in diameter and 8 mm in height) were placed on an Instron machine (JH Ltd., CMT4202) and subjected to slow compression at a rate of 1 mm/min. The compression modulus was calculated by plotting the stress-strain curve based on the recorded compression distance and the corresponding stress at 10 % strain.

Turbidity. A total of 200 μL of pre-gel was pipetted into a 96-well plate. Absorbance at 450 nm was measured every minute for 1 h at 37 °C using a spectrophotometer. The results were normalized against a phosphate buffer solution (PBS) control group to calculate the normalized absorbance using the following formula:

$$NA = \frac{R - R_{min}}{R_{max} - R_{min}}$$

where R represents the absorbance reading at a selected time point, Rmin is the minimum absorbance reading, and Rmax is the maximum absorbance reading.

Nanoindentation: The mechanical properties of the hydrogel were assessed using a Piuma Nanoindenter (Optics11) [27]. A probe with a spring constant of 0.49 N/m and an indentation radius of 31 μm was used under conditions where the cylindrical hydrogel was flattened and immersed in PBS at RT. The indentation was depth-controlled (10 μm), with loading and unloading times set to 2 s. The Young's modulus was calculated based on the load-displacement curve using the Hertz spherical indentation model in Piuma software (V3.3.0).

SEM analysis. The hydrogel samples were prepared in cylindrical shapes with a diameter of 4 mm and a height of 10 mm. After preparation, the samples were lyophilized and subsequently crushed into smaller particles. The crushed samples were coated with a layer of platinum and examined using a scanning electron microscope (Hitachi, S-3400N) to assess their surface morphology.

Isolation of primary hepatocytes. The perfusion solutions were prepared as described [4,5]. 500 mL of Perfusion Solution I and Perfusion Solution II were pre-warmed in a 39 °C water bath. A peristaltic pump (Kamoer, KXP100-GB) was connected to perfuse 100–200 mL of PBS at a flow rate of 5–10 mL/min. PBS was replaced with Perfusion Solution I to fill the cannula and remove air bubbles. A 4-week-old C57BL/6 or nude mouse (according to experiment design) was euthanized and fixed. The abdominal hair was cleaned with 70 % ethanol, and a U-shaped incision was made to open the abdominal cavity, exposing the portal vein. The inferior vena cava was exposed by cutting the diaphragm and ligated, and a needle was inserted, with sutures used to secure the infusion needle. The hepatic portal vein was cut. The vessel was perfused with Perfusion Solution I for 10–15 min, which was followed by Perfusion Solution II supplemented with collagenase IV (Sigma, C4-BIOC), for 10 min. A cotton swab indentation indicated complete digestion as the liver gently swelled. The liver was then removed and placed in a dish containing Perfusion Solution II without collagenase IV. The gallbladder was excised, and liver lobes were separated. The tissue was filtered through a 100-μm mesh, and the filtrate was transferred into two 50 mL centrifuge tubes. Centrifugation was performed at 50 g for 2 min to pellet the hepatocytes. Sedimentary cells were washed with Perfusion Solution II, centrifuged at 50 g for 2 min, and repeated 3–4 times. The hepatocytes were resuspended in 30 mL of advanced DMEM/F12 medium (Thermo Fisher, 12634028). Cell viability was assessed using Trypan Blue and a hemocytometer (Sigma, Z359629).

Organoid cultures. HO medium consisted of advanced DMEM/F12 with HEPES (Sigma, 137270), Glutamax (Gibco, 35050061), and penicillin/streptomycin (KeyGEN, KGL2303-100), 50 ng/mL Rspondin-1 (PeproTech, 315-32), 2 % B-27 (Gibco, 17504044), 50 ng/mL EGF (Gibco, PMG8045), 1.25 mM N-acetylcysteine (Sigma, A0737), 10 nM gastrin (Sigma, 14459), 3 μM CHIR99021 (Sigma, AML1046), 25 ng/mL HGF (Sigma, 15234), 50 ng/mL FGF7 (Sigma, 14178), 50 ng/mL FGF10 (Sigma, 14165), 1 μM A83-01 (Sigma, AML0788), 10 mM niacinamide (Sigma, 1462006), and 10 μM γ-27632 (MCE, 146986-50-7) [4,7]. The isolated hepatocytes were filtered through a 70-μm mesh (Biosharp, BS-70-XBS) and resuspended in cold, advanced DMEM/F12 medium [28]. After counting, the cells were mixed with the pre-gel and cultured in a 24-well plate at a density of 20,000–50,000 cells per well. The dECM pre-gel and matrix gel underwent gelation in a 37 °C incubator, while the dECM-GelMA pre-gel was gelled using 405 nm blue light (6W) for 30 s. After gelation, HO medium was added, with medium changes on day 2 and subsequently every 3 days.

Immunofluorescence staining and imaging. After centrifugation (100×*g*, 4 °C, 5 min), the pellet of organoids was fixed in 4 % PFA solution for 30–60 min. To block and permeabilize the organoids, 1 mL of Triton X-100 and 2 g of Bovine Serum Albumin (ALB) (MCE, 9048-46-8) were added to 1 L of PBS to prepare the organoid washing buffer (OWB) [29]. The fixed organoids were permeabilized with OWB for 20 min. Primary antibodies, including anti-AFP (Abcam, ab284388), anti-Albumin (Abcam, ab207327), anti-beta catenin (Abcam, ab32572), anti-Cytochrome P450 1A2 (Abcam, ab314666), anti-HNF-4-alpha (Abcam, ab41898), anti-Ki67 (Abcam, ab279653), anti-LGR5 (Abcam, ab75850), and anti-Nanog (Abcam, ab214549) were incubated overnight at 4 °C with OWB (1:100 dilution) while gently rotating (60 rpm) [30]. After extensive washing, secondary antibodies (Servicebio, GB22301, GB22303) were incubated overnight at 4 °C with OWB (1:200 dilution) while gently rotating (60 rpm). Subsequently, nuclear staining (KeyGEN, KGA215) was performed. The prepared organoids were transferred to confocal dishes and observed using a confocal microscope (Zeiss, LSM900).

Reprogramming of primary hepatocytes. Plat-E cells (MINGZHOUBIO, MZ8294) at 80 % confluency, were transfected with FugeneHD transfection reagent (Promega, E2311) using the retroviral vector containing murine Oct4, Sox2, Klf4, and c-Myc sequences [31,32]. After 48 h, the virus-containing supernatant was added to a primary hepatocyte culture plate containing 4 μg/mL polybrene (MCE, 28728-55-4), and centrifuged at 2000 rpm for 90 min. Following two rounds of viral infection (once per day), the infected primary hepatocytes were dissociated into single cells and seeded into Matrigel (Corning, 354230) for intestinal organoid culture as described above [33].

Genomics analysis. Cultured organoids were lysed using protein enzymolysis and manual disruption. High quality of RNA was extracted using Trizol reagent (KeyGEN, KGA1201), formyl trichloride and isopropanol, confirmed using 2100 RNA Nano 6000 Assay Kit (Agilent Technologies). Enriched mRNA was fragmented and subjected to reverse transcription. The amplified cDNA was sequenced using Illumina HiSeq2500 (Illumina) with a read length of 100 bp. GSEA (Gene Set Enrichment Analysis), KEGG (Kyoto Encyclopedia of Genes and Genomes) and Hierarchical Cluster analysis were conducted on Solargen

omics.com (ANOROAD) [34,35].

2.3. Hepatectomy and transplantation

Sixty male nude mice, aged 8–10 weeks, were randomly divided into three groups and anesthetized with isoflurane until loss of consciousness [7,36]. Subsequently, the control group underwent hepatic left medial lobectomy; the control group received hepatic left medial lobectomy followed by the injection of 50 μL AHdECM-GM pre-gel (containing 40,000 untreated HOs) into the margin of the remnant liver; and the THBS1 group received hepatic left medial lobectomy followed by the injection of 50 μL AHdECM-GM pre-gel (containing 40,000 THBS1-treated HOs) into the margin of the remnant liver. The mice revived in thermotank. Fourteen days later, the surviving mice were euthanized for histological analysis.

2.4. Liver function analysis

Blood samples collected from the nude mice were analyzed using an automatic biochemical analyzer at Nanjing First Hospital. The levels of total protein (TB), ALB, globulin (GLB), alanine aminotransferase (ALT), aspartate aminotransferase (AST), alkaline phosphatase (ALP) and γ-glutamyl transferase (GGT).

2.5. Statistical analysis

Data are presented as mean ± standard error of the mean. Differences between the experimental groups were analyzed using two-sided *t*-test or one-way analysis of variance. A p-value of ≤0.05 was considered statistically significant. Statistical analysis was performed on GraphPad Prism (v. 9.0).

3. Results

3.1. Fabrication of liver decellularized extracellular matrix (dECM) hydrogel and culture of hepatic organoids (HOs)

To investigate the role of THBS1 in ECM remodeling while ensuring that the stem cell microenvironment closely resembles native tissue and maintains the safety of in vivo transplantation, we developed a photo-polymerizable dECM hydrogel with a stable composition designed to support HOs [13,37]. Key design features of this hydrogel include: (1) providing proteolytic cleavage sites for matrix metalloproteinases (MMPs) and focal adhesion kinase (FAK) activated by THBS1, facilitating hydrogel softening; (2) controllable blue-light crosslinking and mechanical adjustment of hydrogel stiffness throughout the culture process; (3) ECM adhesion sites that promote HO growth and replicate the characteristics of native ECM; (4) stable protein composition confirmed by mass spectrometry when compared to Matrigel; and (5) safety and operability for transplantation.

As a tissue-specific material, the composition and properties of dECM depend on the source animal, tissue type, and decellularization strategy [14]. Although dECM shows promise as a substitute for Matrigel in organoid research, there is no standardized decellularization process for

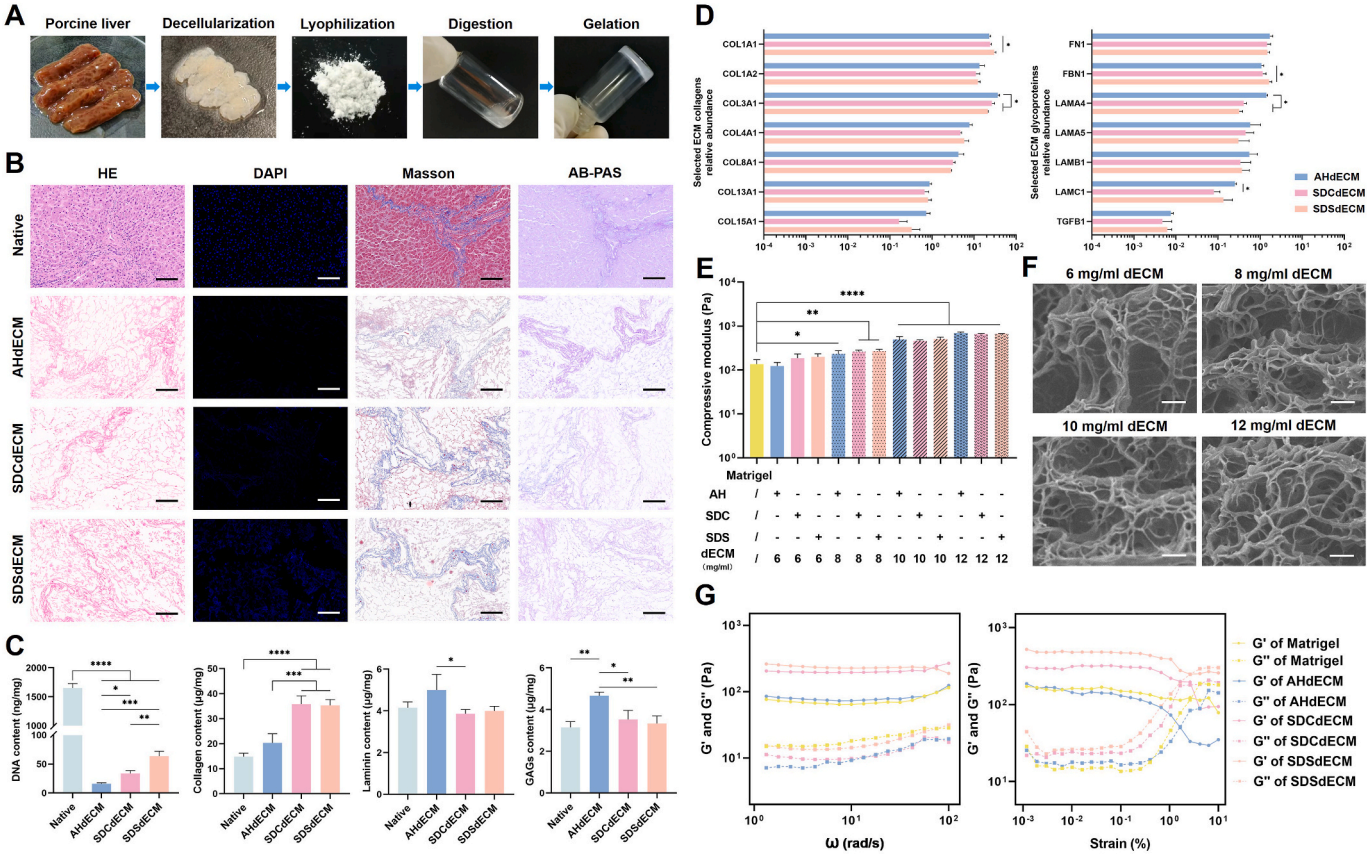

Fig. 1. Fabrication and characterization of liver dECM. A Key steps in the preparation of dECM materials. **B** Histochemistry and immunofluorescence staining of decellularized tissues including HE, DAPI, Masson and AB-PAS. Scale bar = 100 μm. **C** Quantitative analysis of DNA residue and typical ECM proteins in decellularized tissues. Mean ± S.D. ($N = 3$). One-way ANOVA. $^{*}P < 0.05$, $^{**}P < 0.01$, $^{***}P < 0.001$, and $^{****}P < 0.0001$. **D** iTRAQ protein identification and quantification of main ECM proteins in decellularized tissues. Mean ± S.D. ($N = 3$). One-way ANOVA. $^{*}P < 0.05$. **E** Compressive modulus of dECM gels of different decellularization strategies and dECM concentrations. Mean ± S.D. ($N = 3$). Two-sided *t*-test. $^{*}P < 0.05$, $^{**}P < 0.01$, and $^{****}P < 0.0001$. **F** SEM images of dECM hydrogels with varied concentrations. Scale bar = 10 μm. **G** Frequency-sweep and strain-sweep of dECM hydrogels.

HOs. Thus, this study integrated three established methods for decellularizing porcine liver: alcohol-hexane (AH), ionic detergent sodium deoxycholate (SDC), and nonionic detergent sodium dodecyl sulfate (SDS) to compare the diversity of ECM proteins following decellularization.

The preparation of the dECM hydrogel involved five steps: tissue acquisition, decellularization, lyophilization, digestion, and gelation (Fig. 1A). Initially, qualitative analyses of decellularized tissues were conducted using tissue section staining and fluorescence staining (Fig. 1B). Hematoxylin and eosin (HE) staining confirmed the retention of ECM structural proteins, while DAPI staining indicated the successful removal of cells and nuclei. Masson's trichrome staining verified the presence of collagen fibers in the connective tissue, and Alcian blue-periodic acid-Schiff (AB-PAS) staining demonstrated the preservation of glycosaminoglycans (GAGs) and various collagen types. Notably, qualitative analysis illustrated the distinct characteristics of the three decellularization reagents and their effects on ECM components [15].

To compare the outcomes of the three decellularization strategies quantitatively, we analyzed the specific components of decellularized tissues using micro and conventional spectrophotometry (Fig. 1C). Results for DNA residues indicated that while the DNA content in AHdECM and SDCdECM met standards (≤50 ng/mg) [38]. The AHdECM exhibited a significantly higher DNA and cell removal rate than the other two groups, which was corroborated by DAPI staining results (Fig. 1C). Correspondingly, collagen content in the AHdECM was significantly lower than that in the other groups. However, the AHdECM outperformed SDC in retaining laminin, a critical adhesion site for stem cell growth [38,39]. Additionally, GAG content in the dECM was

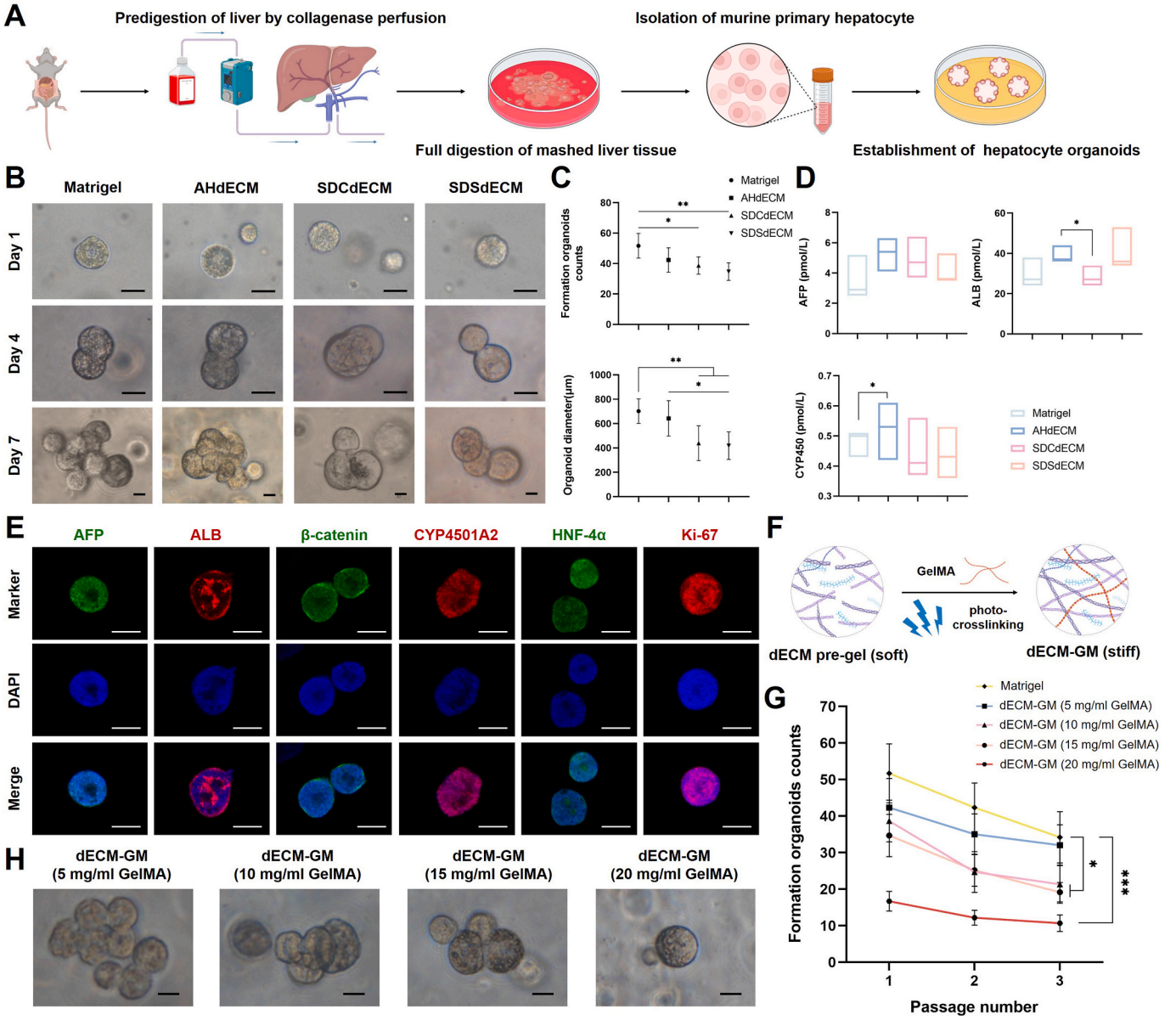

Fig. 2. Culture of HOs within dECM & **dECM-GM. A** Flow diagram shows the isolation of primary hepatocytes via perfusion & digestion method and establishment of HOs culture in vitro. **B** Typical bright field images of formed spheroids and HOs in Matrigel and dECM hydrogels (6 mg/ml) of different decellularization strategies. Scale bar = 100 μm. **C** Calculated formed HOs per field of view at 10 × and averaged organoids diameters on day 7. Mean ± S.D. ($N = 12$). One-way ANOVA. $^{*}P < 0.05$ and $^{**}P < 0.01$. **D** Measured concentration of proteins involved in liver function. Mean ± S.D. ($N = 3$). One-way ANOVA. $^{*}P < 0.05$. **E** Immunofluorescence staining of HOs in AHdECM on day 5, including AFP, ALB, β-catenin, CYP4501A2, HNF-4α, and Ki-67. Scale bar = 100 μm. **F** Flow diagram demonstrates the network of dECM-GM hydrogel. **G** Calculated formed HOs per field of view at 10 × after passaging in dECM-GM. Mean ± S.D. ($N = 6$). Two-sided *t*-test. $^{*}P < 0.05$ and $^{***}P < 0.001$. **H** Typical bright field images of formed spheroids and HOs in AHdECM-GM.

significantly higher than in the other two groups, reflecting the distinct effects of the three main decellularization reagents. To further quantify the differences in ECM components and initiate HO culture experiments, we conducted LC-MS/MS to assess the relative abundance of typical ECM proteins (Fig. 1D). The mass spectrometry results further revealed significant heterogeneity in the quantities of ECM proteins and growth factors among batches of Matrigel compared to dECM hydrogels (Fig. S1). We also compared the compressive modulus of dECM hydrogels to that of Matrigel (Fig. 1E), and typical scanning electron microscopy (SEM) images confirmed the porous network within dECM hydrogels (Fig. 1F). Rheological analysis indicated that different decellularization strategies imparted distinct mechanical properties to the dECM hydrogels (Fig. 1G).

Next, we validated the culturing capability of the dECM hydrogels for HOs. Primary hepatocytes were isolated from C57BL/6 mice using a perfusion and digestion method and were incubated in an HO expansion medium in vitro (Fig. 2A) [4]. Similar to Matrigel, the dECM group required temperature-induced protein crosslinking (Fig. S2). Notably, during the 12–36 h, primary hepatocytes in dECM hydrogels proliferated and self-assembled into spheroids, akin to those observed in the Matrigel group. Between 48 and 72 h, budding of spheroids and asymmetric expansion and maturation of the organoids were noted in the Matrigel group (Fig. 2B). Subsequently, hepatocyte spheroids in dECM hydrogels displayed budding and asymmetric expansion by 96 h of culture (Fig. 2B) [40]. By day 7, spheroid-like HOs were evident in dECM hydrogels, similar to the control group. Statistical analysis on day 7 revealed that the number of organoids formed in SDCdECM and SDSdECM was significantly lower than in the control group (Fig. 2C) [41,42]. The protein activity and protein concentration of the cultures were also measured to reflect the liver function of HOs (Fig. 2D). AHdECM showed no significant difference in organoid size and higher CYP450 activity compared to the control group, suggesting that ECM characteristics resulting from different decellularization strategies may differentially influence stem cell proliferation and organoid formation. Immunofluorescence analysis further validated and examined the function and proliferation status of the HOs, including markers for hepatocyte function (ALB and CYP4501A2), hepatocyte-specific markers (AFP and HNF-4α), and proliferation markers (Ki-67 and β-catenin) (Fig. 2D). Quantification of fluorescence staining results provided additional insights (Fig. S3).

To replicate the mechanical strength of native tissue ECM, we incorporated a GelMA blue-light crosslinking system validated for organoid culture (Fig. 2E). The crosslinking networks between ECM proteins and GelMA molecules serve as potential MMP targets [43]. Results from compression tests on the elastic modulus of pre-gelled decellularized materials at different concentrations demonstrated a stepwise increase in strength after gelation (Fig. 2F). The elastic modulus, or stiffness, of the ECM significantly influences key cellular

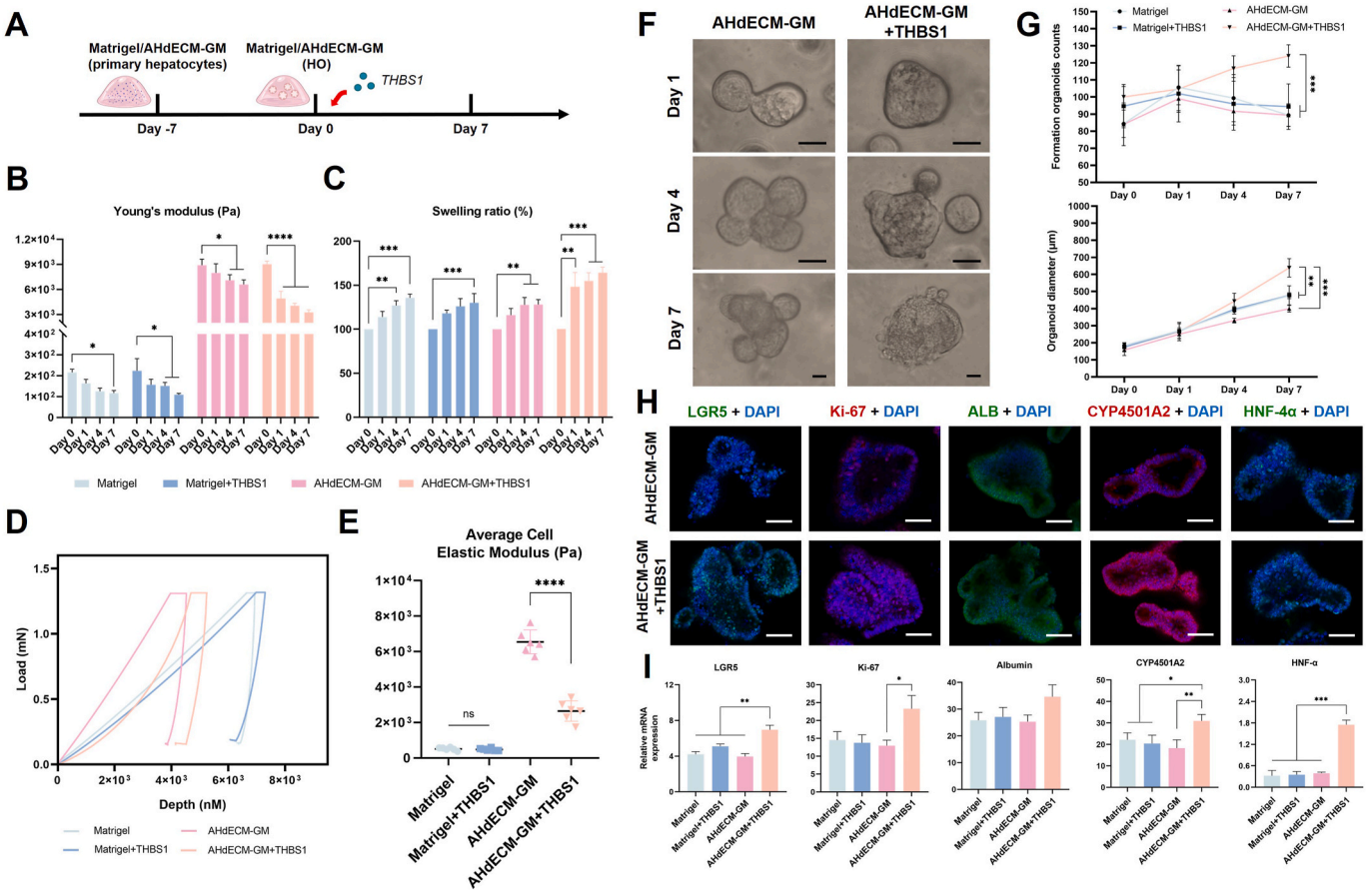

Fig. 3. THBS1 endows dECM-GM with dynamic structural characteristics and affects HOs maturation. A Schematic shows the timing and treatment in AHdECM-GM + THBS1 group. **B** Elastic modulus of Matrigel, Matrigel + THBS1, AHdECM-GM, and AHdECM-GM + THBS1 on day 0, 1, 4, and 7. Mean ± S.D. ($N = 3$). One-way ANOVA. $^{*}P < 0.05$, $^{**}P < 0.01$, $^{***}P < 0.001$, and $^{****}P < 0.0001$. **C** Swelling ratio of different groups on day 0, 1, 4, and 7. Mean ± S.D. ($N = 3$). One-way ANOVA. $^{*}P < 0.05$ and $^{****}P < 0.0001$. **D** Representative indentation curves on day 0, 1, 4 and 7. **E** The elastic modulus of hepatocytes within HOs in touch with the matrixes. Mean ± S.D. ($N = 6$). Two-sided *t*-test. $^{****}P < 0.0001$. **F** Typical bright field images of HOs. Scale bar = 100 μm. **G** Calculated matured HOs per field of view at 10 × ($N = 6$) and averaged organoids diameters ($N = 12$) on day 0, 1, 4, and 7. Mean ± S.D. One-way ANOVA. $^{**}P < 0.01$ and $^{***}P < 0.001$. **H** Immunofluorescence staining of HOs on day 5, including LGR5, Ki-67, ALB, CYP4501A2, and HNF-4α. Scale bar = 100 μm. **I** Relative mRNA expression by quantitative real-time PCR of selected genes. Gene expression is relative to β-Actin gene. Mean ± S.D. ($N = 3$). One-way ANOVA. $^{*}P < 0.05$, $^{**}P < 0.01$, and $^{***}P < 0.001$.

processes such as growth, proliferation, migration, differentiation, and organoid formation, making it a critical metric in biomaterial evaluation [16]. The inclusion of the GelMA crosslinking system provided the dECM hydrogels with tunable mechanical properties (Fig. S4). Primary hepatocytes were cultured within the decellularized extracellular matrix -gelatin methacrylate (dECM-GM) to initiate organoid culture (Fig. 2H). In terms of organoid count, dECM-GM (5, 10, and 15 mg/ml GelMA) exhibited comparable efficacy to Matrigel (Fig. 2G).

3.2. Effect of Thrombospondin-1 (THBS1) on mechanical characteristics of dECM network and growth/differentiation status of hepatocyte organoids (HOs)

The culture medium for dECM-GM (6 mg/ml AHdECM and 5 mg/ml GelMA) were added with 100 U/ml THBS1, with medium changes every two days (Fig. 3A) [17,43]. Characterization of the dECM-GM post--treatment revealed that THBS1 induced significant alterations in the ECM strength and swelling ratio (Fig. 3B–C). Notably, dECM-GM + THBS1 exhibited varying stiffness on days 1, 4, and 7, contrasting with the initial stiffness values, while no such changes were observed in the other groups (Fig. 3B) [44]. These findings suggest that THBS1 imparts time-dependent mechanical behavior and viscoelasticity to the hydrogel, characterized by significant stress relaxation after swelling deformation.

To further explore the hepatocyte-ECM interactions, we measured the elastic modulus of hepatocytes within the HOs in contact with the matrices using nanoindentation techniques (Fig. 3D) [45]. We observed a significantly decreased cellular elastic modulus, a key parameter related to adhesion and migration behaviors (Fig. 3E). This supports our hypothesis that THBS1 regulates the stiffness and mechanical dissipation properties of the ECM hydrogel network, influencing the adaptation and remodeling processes between the organoid microenvironment and the surrounding ECM proteins [30]. This dynamic structural feature bestows the system with viscoelastic behavior at the cellular level. However, when we directly added MMP-2 and MMP-9 at the same concentrations to the AHdECM-GM system, nanoindentation did not reveal matrix dynamic changes similar to those induced by THBS1, demonstrating that this continuous variation in cellular forces is generated by the action of THBS1 on hepatocytes (Fig. S5).

Subsequently, we characterized how the structural variations conferred by THBS1 to the hydrogel influence and regulate primary hepatocytes and HOs [46]. Interestingly, the results revealed a steady increase in the number of formed HOs in the THBS1 group over the 7-day observation period, with a significant rise on day 7 compared to the other groups (Fig. 3G). Additionally, the diameter of the HOs showed a noticeable increase on day 7 in the THBS1 group relative to the other groups. To assess THBS1's effects on hepatocyte proliferation and differentiation within the HOs, we performed immunofluorescence analysis, which indicated a significant increase in the proportion of proliferative hepatocytes (Fig. 3H). Quantitative real-time polymerase chain reaction (qPCR) analysis of hepatocyte proliferation and functional markers within the HOs also indicated regulation by THBS1 (Fig. 3I).

To further characterize the effects of differentiation and proliferation under these conditions, we transfected primary hepatocytes with retroviral vectors expressing Oct4, Sox2, Klf4, and c-Myc before organoid culture [32]. Ten days post-transfection, immunofluorescence confirmed the expression of the pluripotent cell marker Nanog in the hepatocytes (Fig. S6). The reprogrammed mouse hepatocytes were subsequently cultured in HOs within dECM-GM. Remarkably, after 7 days, the ratios of AFP+, ALB+, β-catenin+, and HNF-4α+ cells in both the reprogrammed group and the THBS1 group were found to be similar (Fig. S7).

3.3. THBS1 propels stiffness-variation dependent hepatocytes reprogramming by activating yes-associated protein (YAP)

Transcriptomic analysis was performed to elucidate the mechanisms by which THBS1 significantly affects HOs. Previous studies indicate that exosomal THBS1 drives tumor invasion by modifying the ECM through the activation of MMPs and FAK [19,20]. Western blot (WB) analysis confirmed an increase in the expression and activity of phosphorylated MMPs and phosphorylated FAK (Fig. 4A and B). This cell-dependent activation and secretion of MMPs likely explain the changes in ECM hydrogel stiffness and viscoelasticity induced by THBS1.

RNA sequencing revealed substantial changes in hepatocytes following THBS1 treatment within AHdECM-GM (6 mg/ml dECM & 5 mg/ml GelMA), identifying 1606 significantly upregulated and 1421 downregulated genes in the THBS1 group (Fig. S8). Notably, typical hepatic progenitor cell markers such as AFP, EPCAM, WNT2, WNT7a, WNT7b, WNT10a, WNT11, WNT16, NOTCH1, and NOTCH4 were significantly upregulated. Additionally, the mRNA expression of THBS1 itself was notably increased, indicating a positive feedback loop triggered by THBS1-mediated changes in ECM stiffness. The transcription factors KLF4 and SOX2, known for their roles in cell reprogramming, were also significantly upregulated [47,48]. Gene Set Enrichment Analysis (GSEA) identified significantly altered signaling pathways, particularly highlighting the Hippo-YAP pathway and Rho receptors, which serve as key ECM sensors (Fig. 4G). To confirm the role of YAP as an effector in hepatocyte reprogramming induced by ECM stiffness changes, we measured the expression levels of YAP and phosphorylated YAP (Fig. 4H) [33].

The Hippo-YAP signaling pathway is crucial for regulating organ size, stem cell function, tissue growth, and tumorigenesis [49]. The Hippo pathway consists of a series of kinases that negatively regulate the protein stability and nuclear localization of YAP and TAZ. These kinases are modulated by various upstream signals, including G protein-coupled receptors (GPCRs), WNT proteins, cell-cell contacts, and mechanical forces [50]. Previous studies have shown that matrix stiffness promotes liver organoid formation through FAK and YAP [51]. Although stiffer matrices have been associated with enhanced HOs proliferation, we observed a significant increase in the proportion of proliferative hepatocytes within HOs following THBS1 treatment across both ECM environments of varying stiffness (6 mg/ml dECM & 5 mg/ml GelMA; 6 mg/ml dECM & 15 mg/ml GelMA) (Fig. 5B and C) [52].

Subsequently, we applied inhibitors of MMPs, FAK, and the Rho-YAP pathway alongside THBS1 treatment, which led to a significant downregulation of YAP levels compared to the untreated group, further suggesting that the activation of MMPs, FAK, and Rho receptors serves as upstream mediators of YAP in the reprogramming effects induced by THBS1 (Fig. 5D). Moreover, when comparing programmed HOs transfected with Oct4/Sox2/KLF4/c-Myc, THBS1 led to a comparable increase in the ratio of Ki-67+ cells, which was eliminated by the combination with GM6001 (an MMP2 inhibitor), Rhosin (a Rho inhibitor), and Verteporfin (a YAP inhibitor) (Fig. 5E). Although programmed HOs exhibited a significantly higher ratio of Nanog + cells, a critical pluripotency marker, compared to the THBS1 group, the THBS1 group also showed a notable increase in Nanog + cells compared to the control group [53]. These variations in YAP activation and hepatocyte phenotype provide compelling evidence that THBS1 promotes HOs reprogramming via ECM-induced Rho-YAP activation (Fig. 5F).

3.4. THBS1 enhances proliferation and migration of HOs improves liver repair after transplantation into hepatectomy mice

Before conducting transplantation experiments in nude mice, AHdECM-GM was first transplanted under the dorsal skin of C57 mice to evaluate the inflammatory response (Fig. S9A). Immunofluorescence results from AHdECM-GM group exhibited decreased proportion of F4/80^{+} macrophages (Fig. S9B). After several preliminary attempts, we

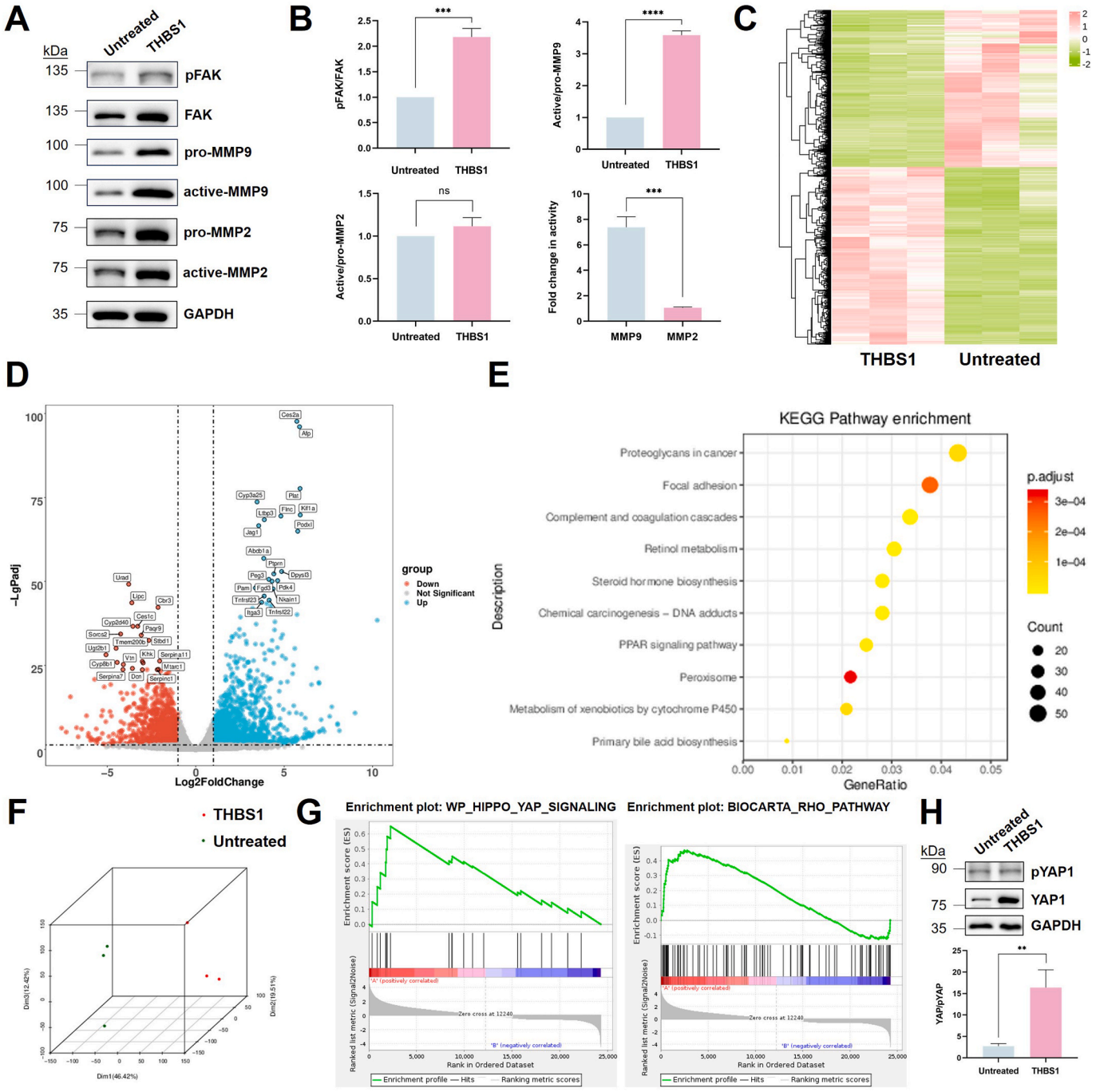

Fig. 4. Transcriptomic signature analysis of HOs in AHdECM-GM and AHdECM-GM + THBS1. **A** Western blot analysis of pFAK, FAK, pro-MMP9, active-MMP9, pro-MMP2, and active-MMP2 from HOs cultured in AHdECM-GM + THBS1. **B** Quantitative analysis of protein's expression based on results from western blot using Image J (2.14.0) and activity using ELISA kits. Mean ± S.D. ($N = 3$). Two-sided t-test. ***$P < 0.001$ and ****$P < 0.0001$. **C** Heat map of expression of differentially expressed genes ordered according to hierarchical clustering. **D** Volcano plot shows top upregulated or downregulated genes. **E** Bubble chart shows results of KEGG pathway enrichment analysis. **F** Principal component analysis of gene expression. **G** Significantly enriched MSigDB gene sets using GSEA. **H** Western blot and quantitative analysis of pYAP1 and YAP. Mean ± S.D. ($N = 3$). Two-sided t-test. **$P < 0.01$.

opted for an injection and in situ blue-light crosslinking transplantation strategy in a 70 % partial hepatectomy model using nude mice, where liver injury induces a series of measurable changes (Fig. 6A) [7,54]. The limited operative space in nude mice rendered patch transplantation impractical. We isolated primary hepatocytes from genetically marked green fluorescent protein (GFP) mice and subjected them to organoid culture with THBS1 treatment to facilitate post-transplantation identification and differentiation [55]. The HOs were encapsulated in AHdECM-GM (1 kPa; 6 mg/ml dECM & 5 mg/ml GelMA) pre-gel.

The sham group only received hepatectomy. THBS1 was not added to AHdECM-GM in the control group. On day 14, the THBS1 group exhibited significantly higher survival rate than the sham group. Analysis of liver and blood samples collected 14 days post-surgery revealed that the liver-to-body weight ratio, total protein (TP), and total bilirubin (TB) levels were significantly higher in the THBS1 group compared to the sham group. In contrast, the control group did not exhibit significant differences from the other two groups (Fig. 6B and C). Additionally, serum albumin (ALB) levels in the THBS1 group were significantly

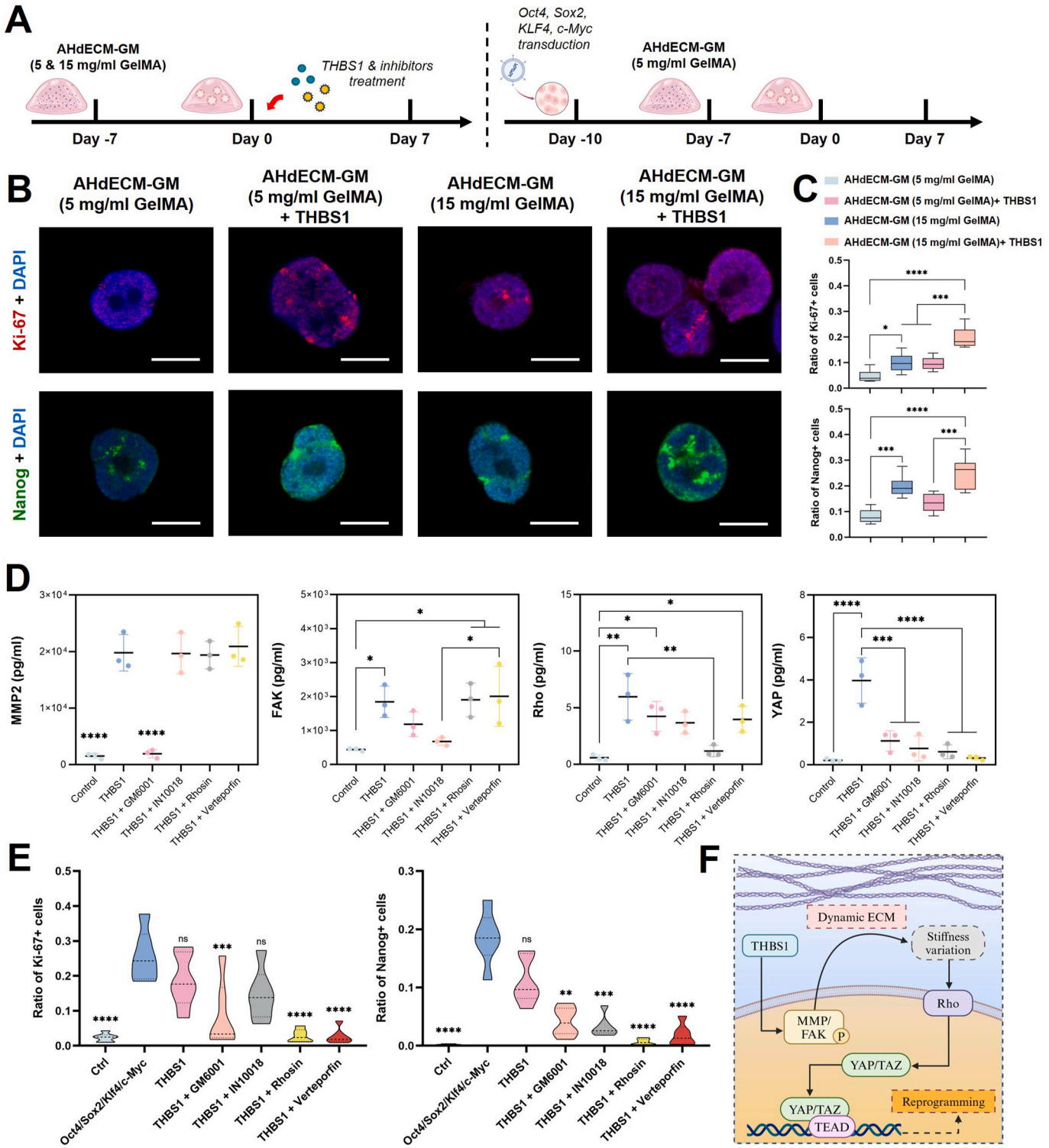

Fig. 5. Activation of Rho-YAP and HOs reprogramming via THBS1-induced ECM variation. A Schematic shows the addition of THBS1 into HOs cultured within AHdECM-GM (6 mg/ml dECM & 5 mg/ml GelMA; 6 mg/ml dECM & 15 mg/ml GelMA) respectively, and the combination with MMPs, FAK, and Rho-YAP pathway inhibitors into HOs cultured within dECM-GelMA hydrogel (left) compared with reprogrammed HOs induced by the transduction of Oct4, Sox2, Klf4, and c-Myc (right). **B** Immunofluorescence staining of Ki-67 and Nanog within HOs. Scale bar = 100 μm. **C** Counted ratio of Ki-67/Nanog + cells within HOs based on the result of immunofluorescence staining. Mean ± S.D. ($N = 6$). One-way ANOVA. $^{*}P < 0.05$, $^{***}P < 0.001$, and $^{****}P < 0.0001$. **D** Detected expression of MMP2, FAK, Rho, and YAP within HOs added with GM6001 (MMP2 inhibitor), IN10018 (FAK inhibitor), Rhosin (Rho inhibitor), and Verteporfin (YAP inhibitor) using ELISA kits. Mean ± S.D. ($N = 6$). One-way ANOVA. $^{*}P < 0.05$, $^{**}P < 0.01$, $^{***}P < 0.001$, and $^{****}P < 0.0001$. **E** Counted ratio of Ki-67/Nanog + cells within HOs added with MMPs, FAK, and Rho-YAP pathway inhibitors and reprogrammed HOs (Oct4/Sox2/Klf4/c-Myc group). Statistical markers show the comparative result between Oct4/Sox2/Klf4/c-Myc group and others. Mean ± S.D. ($N = 6$). Two-sided *t*-test. $^{**}P < 0.01$, $^{***}P < 0.001$, and $^{****}P < 0.0001$. **F** Proposed model of Rho-YAP activation and hepatocyte reprogramming by THBS1-induced ECM variation.

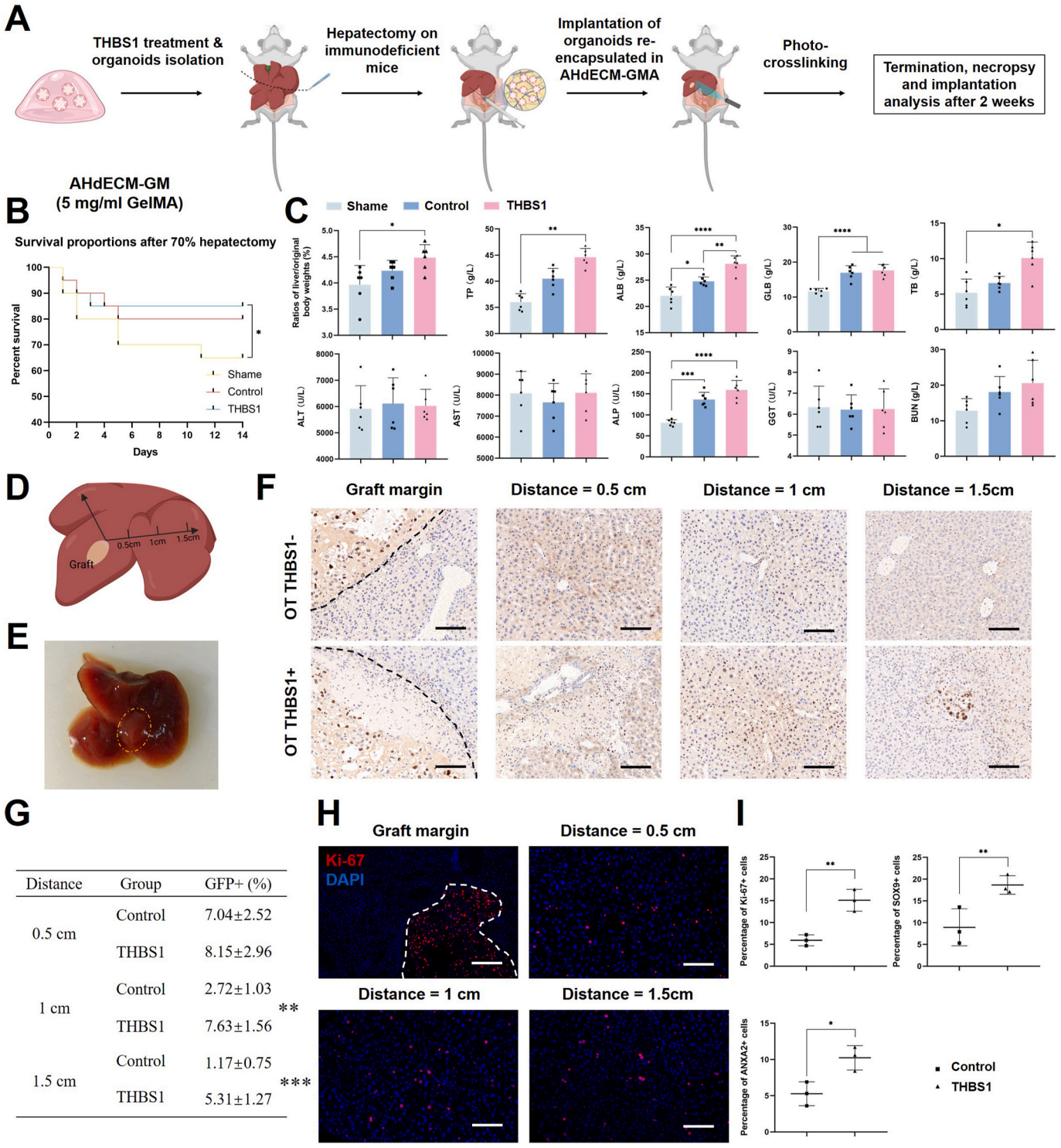

Distance	Group	GFP+ (%)	
0.5 cm	Control	7.04±2.52	
	THBS1	8.15±2.96	
1 cm	Control	2.72±1.03	**
	THBS1	7.63±1.56	
1.5 cm	Control	1.17±0.75	***
	THBS1	5.31±1.27	

Fig. 6. Transplantation of THBS1-treated GFP + HOs into the livers of nude mice receiving 70 % hepatectomy. A Schematic shows the transplantation process using 70 % partial hepatectomy animal model of nude mice. **B** Survival curve of 3 groups after hepatectomy. Mean ± S.D. ($N = 20$). One-way ANOVA. *$P < 0.05$. **C** Detected liver-body-weight ratio and liver-associated serum indexes after 14 days post-transplantation. Mean ± S.D. ($N = 6$). One-way ANOVA. *$P < 0.05$, **$P < 0.01$, ***$P < 0.001$, and ****$P < 0.0001$. **D** Schematic shows the sampling positions equidistant from the graft. **E** A liver harvested from OT THBS1+ group with visible graft at injection site. **F** Histochemistry analysis of tissue sections from sampling positions indicates GFP + donor hepatocytes using antibody to GFP linked to diaminobenzidine. Scale bar = 100 μm. **G** Counted percentage of GFP + cells at different sampling positions. Mean ± S.D. ($N = 6$). Two-sided *t*-test. **$P < 0.01$ and ***$P < 0.001$. **H** Immunofluorescence staining of Ki-67 on tissue sections from sampling positions. Scale bar = 100 μm. **I** Percentage of Ki-67+, SOX9+, and ANXA2+ cells among GFP + donor cells within hepatic lobule-like structures. Mean ± S.D. ($N = 3$). One-way ANOVA. *$P < 0.05$ and **$P < 0.01$.

elevated relative to the other two groups, indicating enhanced recovery of hepatocyte function.

In the livers of mice that received organoid transplants, a transparent tissue at the injection site was clearly distinguishable from the surrounding native tissue (Fig. 6E). The migration capacity of stem cells post-transplantation is a critical indicator of their regenerative potential and homing efficiency. Therefore, we conducted immunohistochemical analysis at varying distances from the transplantation site. The immunohistochemistry results demonstrated that AHdECM-GM hydrogels formed loose lobule-like structures post-transplantation, with residual ECM observed (Fig. 6F).

Statistical analysis of the GFP + cell ratio at different distances indicated that the THBS1 group exhibited significantly greater hepatocyte migration efficiency to distant sites compared to the control group (Fig. 6G). Furthermore, immunofluorescence staining for the proliferation marker Ki-67, the hepatocarcinogenesis marker SOX9 (a downstream target of YAP), and the migration capacity marker ANXA2 revealed that the proportion of Ki-67+ cells in the liver lobule-like structures of the THBS1 group was significantly higher than in the other two groups (Fig. 6I) [56–58].

The proportion of SOX9-positive cells, a marker of hepatocyte reprogramming following liver injury, was also greater in the THBS1 group compared to the control group, suggesting THBS1-mediated reprogramming effects and its role in promoting liver regeneration (Fig. S10). Notably, ANXA2, a newly identified marker associated with migratory hepatocytes during liver regeneration, showed a significantly higher proportion of positive cells in the liver lobule-like structures of the THBS1 group.

4. Discussion

Organoids have demonstrated significant potential for regenerative applications; however, a major challenge lies in the reliance on mouse tumor-derived ECM extracts to initiate and expand organoid cultures [59]. The presence of tumor-derived small molecular contaminants in these extracts not only restricts the clinical applicability of organoids but also complicates the in vitro study of stem cell organogenesis regulation [60,61]. In contrast, dECM derived from human or porcine liver present an attractive alternative. Although previous studies have reported that liver ECM hydrogels support the culture of HOs or cholangiocyte organoids, inconsistencies in decellularization techniques have led to high variability in dECM composition, undermining the reliability of findings [62]. Our study is the first to systematically compare the effects of commonly used liver decellularization strategies on the properties of dECM materials and the efficacy of organoid culture. Furthermore, we refined the hydrogels using a GelMA crosslinking system, also derived from natural proteins, to create tissue-specific and bioactive microenvironments with adjustable mechanical properties.

Numerous studies have explored the relationship between the in vitro regulation of stem cells within organoids and their regenerative potential [63]. Emerging evidence suggests that ECM stiffness-mediated by stress sensors within the Hippo-YAP signaling pathway–plays a pivotal role in the regulation of stem cells and organoid growth [64,65]. In our work, we introduced a viscoelastic, dynamic natural tissue hydrogel that allows for stiffness adjustments during culture, achieved by incorporating exogenous THBS1 into liver dECM hydrogels. This approach marks a departure from traditional static culture methods, providing deeper insights into the mechanical responses and in vitro regulation of HOs. THBS1, initially identified as a glycoprotein in platelets, has since been recognized as an adhesion-related protein that influences various cell-ECM adhesion processes [66]. Prior research has indicated that THBS1 promotes monocyte and T lymphocyte adhesion through vascular cell adhesion molecule induction and integrin regulation, respectively [67]. Additionally, THBS1 has been implicated in facilitating tumor cell invasion and metastasis via MMP activation, resulting in unstable cell adhesion [68,69]. Our research elucidates that THBS1 can modulate the stiffness and mechanical dissipation properties of natural ECM hydrogel networks, influencing the adaptive adhesion and migration processes between organoids and surrounding ECM proteins. This interaction generates mechanical signals that stem cells can perceive, introducing the concept of ECM stiffness variation as a regulatory factor for HOs' growth. Although our findings demonstrate changes in ECM stiffness around organoids through nanoindentation, further investigations are necessary to quantify THBS1-mediated activation of MMPs and FAK, along with alterations in ECM mechanical signaling and the Rho-YAP response.

Importantly, THBS1-mediated in vitro regulation induced a reprogramming-like effect in primary hepatocytes, thereby promoting organoid proliferation and tissue regeneration post-transplantation. Adult stem cells (ASCs) have traditionally been favored as seed cells for organoid cultures due to their accessibility and shorter cultivation periods compared to iPSCs [70,71]. While organoids derived from ASCs show enhanced proliferation, their differentiation lineage remains highly tissue-specific. For example, intestinal stem cells from the base of intestinal villi exclusively produce mucosal epithelial cells through organoid culture, lacking the ability to generate stromal cells. In contrast, iPSC-derived organoids can reselect differentiation pathways and produce stromal cells [72,73]. This pluripotency renders iPSCs ideal seed cells for liver regeneration and repair, as they can differentiate into various cell types necessary for forming hepatic lobule structures [74–76]. Our study is the first to demonstrate that HOs derived from primary hepatocytes exhibit significant upregulation of KLF4 and SOX2, alongside organoid-level regulation following Hippo-YAP pathway activation in response to ECM stiffness changes, confirming the sustained initiation of reprogramming [77].

We successfully performed safe and effective injection transplantation of HOs containing reprogrammed liver progenitor cells into the residual liver of a hepatectomy-induced injury animal model [78,79]. Compared to previously reported methods such as patch grafting, vascular propagation, and ectopic transplantation, injection transplantation emerges as the most straightforward and least damaging approach for small animal hepatectomy models [7,13,54]. Our findings also demonstrate the formation of in situ hepatic lobule-like structures and ectopic migration following HOs transplantation. Evidence of enhanced liver regeneration is supported by metrics such as liver weight gain and improved liver synthetic function. However, due to current technological limitations, we were unable to ascertain whether reprogrammed liver organoids can fully differentiate or assemble into functional structures, including central veins, hepatic sinusoids, and bile canaliculi within the hepatic lobule-like structures. Also, long-term monitoring is necessary to confirm that organoid transplantation following reprogramming does not elevate the risk of cancer [8,9]. Additionally, we did not separately explore the respective contributions of AHdECM-GM and HOs in liver repair. Although dECM scaffolds are considered beneficial for interstitial recovery, more in-depth studies are required to be conducted in models of varying degrees of liver injury [54].

CRediT authorship contribution statement

Zi-Yan Xu: Writing – review & editing, Writing – original draft, Visualization, Validation, Supervision, Software, Resources, Project administration, Methodology, Investigation, Funding acquisition, Formal analysis, Data curation, Conceptualization. **Min Wang:** Writing – original draft, Visualization, Methodology, Investigation, Conceptualization. **Jing-Yan Shi:** Methodology, Investigation, Formal analysis, Conceptualization. **Ye Liu:** Methodology, Investigation. **Chao Yu:** Validation, Software. **Xin-Yi Zhang:** Software, Methodology. **Chen-Wei Zhang:** Resources, Methodology. **Qi-Feng He:** Visualization, Resources. **Chao Pan:** Formal analysis, Investigation. **Jin Zhou:** Validation, Supervision, Resources. **Hua Xiao:** Writing – review & editing, Data curation, Conceptualization. **Hong-Yong Cao:** Writing – review &

editing, Resources, Project administration, Funding acquisition, Conceptualization. **Yong Ma:** Writing – review & editing, Project administration, Methodology, Investigation, Funding acquisition, Data curation, Conceptualization.

Ethical committee

Experimental Animal Ethics Committee of Nanjing Hospital Affiliated to Nanjing Medical University.

Publishing ethics

The study was approved by the Experimental Animal Ethics Committee of Nanjing Hospital Affiliated to Nanjing Medical University. All animal experiments were carried out under the conditions of animal ethics.

Funding

This work was supported by the China Postdoctoral Science Foundation [grant number 2022M721667], Nanjing Health Technology Development Project [grant number ZKX23031 & YKK24119], Jiangsu Provincial Natural Science Foundation [grant number BK20240259] and National Natural Science Foundation of China [grant number 82400645], Hubei Chen Xiaoping science and Technology Development Foundation [grant number CXPJJH12000009-08].

Declaration of competing interest

The authors declare that they have no known competing financial interests or personal relationships that could have appeared to influence the work reported in this paper.

Appendix A. Supplementary data

Supplementary data to this article can be found online at https://doi.org/10.1016/j.mtbio.2025.101700.

Data availability

Data will be made available on request.

References

[1] A.W. Duncan, C. Dorrell, M. Grompe, Stem cells and liver regeneration, Gastroenterology 137 (2) (2009) 466–481.
[2] G.K. Michalopoulos, B. Bhushan, Liver regeneration: biological and pathological mechanisms and implications, Nat. Rev. Gastroenterol. Hepatol. 18 (1) (2021) 40–55.
[3] S.R. Lieber, T.D. Schiano, R. Rhodes, Should living donor liver transplantation be an option when deceased donation is not? J. Hepatol. 68 (5) (2018) 1076–1082.
[4] H. Hu, et al., Long-term expansion of functional mouse and human hepatocytes as 3D organoids, Cell 175 (6) (2018) 1591–1606.e19.
[5] L. Broutier, et al., Culture and establishment of self-renewing human and mouse adult liver and pancreas 3D organoids and their genetic manipulation, Nat. Protoc. 11 (9) (2016) 1724–1743.
[6] M. Huch, et al., In vitro expansion of single Lgr5+ liver stem cells induced by Wnt-driven regeneration, Nature 494 (7436) (2013) 247–250.
[7] W. Zhang, et al., Patch grafting, strategies for transplantation of organoids into solid organs such as liver, Biomaterials 277 (2021) 121067.
[8] S. Kim, et al., Tissue extracellular matrix hydrogels as alternatives to Matrigel for culturing gastrointestinal organoids, Nat. Commun. 13 (1) (2022) 1692.
[9] M.K. Kim, W. Jeong, H.W. Kang, Liver dECM-gelatin composite bioink for precise 3D printing of highly functional liver tissues, J. Funct. Biomater. 14 (8) (2023).
[10] H. Lee, et al., Development of liver decellularized extracellular matrix bioink for three-dimensional cell printing-based liver tissue engineering, Biomacromolecules 18 (4) (2017) 1229–1237.
[11] T. Tadokoro, et al., Human iPSC-liver organoid transplantation reduces fibrosis through immunomodulation, Sci. Transl. Med. 16 (757) (2024) eadg0338.
[12] S. Kim, et al., Tissue extracellular matrix hydrogels as alternatives to Matrigel for culturing gastrointestinal organoids, Nat. Commun. 13 (1) (2022) 1692.
[13] T. Wang, et al., Injectable decellularized extracellular matrix hydrogel promotes salivary gland regeneration via endogenous stem cell recruitment and suppression of fibrogenesis, Acta Biomater. 169 (2023) 256–272.
[14] L. Zhu, et al., Decellularized extracellular matrix for remodeling bioengineering organoid's microenvironment, Small 19 (25) (2023) e2207752.
[15] M. Brown, et al., Decellularized extracellular matrix: new promising and challenging biomaterials for regenerative medicine, Biomaterials 289 (2022) 121786.
[16] C. Liu, et al., Engineering the viscoelasticity of gelatin methacryloyl (GelMA) hydrogels via small "dynamic bridges" to regulate BMSC behaviors for osteochondral regeneration, Bioact. Mater. 25 (2023) 445–459.
[17] B. Wu, et al., Stiff matrix induces exosome secretion to promote tumour growth, Nat. Cell Biol. 25 (3) (2023) 415–424.
[18] W. Liu, et al., Decellularized extracellular matrix materials for treatment of ischemic cardiomyopathy, Bioact. Mater. 33 (2024) 460–482.
[19] S. Patwardhan, et al., ECM stiffness-tuned exosomes drive breast cancer motility through thrombospondin-1, Biomaterials 279 (2021) 121185.
[20] M. Omatsu, et al., THBS1-producing tumor-infiltrating monocyte-like cells contribute to immunosuppression and metastasis in colorectal cancer, Nat. Commun. 14 (1) (2023) 5534.
[21] Q. Mao, et al., Fabrication of liver microtissue with liver decellularized extracellular matrix (dECM) bioink by digital light processing (DLP) bioprinting, Mater Sci Eng C Mater Biol Appl 109 (2020) 110625.
[22] L.A. Milton, et al., Liver click dECM hydrogels for engineering hepatic microenvironments, Acta Biomater 185 (2024) 144–160.
[23] M.M. De Santis, et al., Extracellular-matrix-Reinforced bioinks for 3D bioprinting human tissue, Adv Mater 33 (3) (2021) e2005476.
[24] J. Liu, et al., iTRAQ-facilitated proteomic profiling of anthers from a photosensitive male sterile mutant and wild-type cotton (Gossypium hirsutum L.), J Proteomics 126 (2015) 68–81.
[25] P. Chu, et al., iTRAQ-based quantitative proteomics analysis of Brassica napus leaves reveals pathways associated with chlorophyll deficiency, J Proteomics 113 (2015) 244–259.
[26] Z.Y. Xu, et al., Extracellular matrix bioink boosts stemness and facilitates transplantation of intestinal organoids as a biosafe Matrigel alternative, Bioeng Transl Med 8 (1) (2023) e10327.
[27] S.A. Xie, et al., Matrix stiffness determines the phenotype of vascular smooth muscle cell in vitro and in vivo: role of DNA methyltransferase 1, Biomaterials 155 (2018) 203–216.
[28] Y. Guan, et al., A human multi-lineage hepatic organoid model for liver fibrosis, Nat. Commun. 12 (1) (2021) 6138.
[29] J.F. Dekkers, et al., High-resolution 3D imaging of fixed and cleared organoids, Nat. Protoc. 14 (6) (2019) 1756–1771.
[30] Z. Wen, et al., THBS1-Mediated degradation of collagen via the PI3K/AKT pathway facilitates the metastasis and poor prognosis of OSCC, Int. J. Mol. Sci. 24 (17) (2023).
[31] T. Chen, et al., E-cadherin-mediated cell-cell contact is critical for induced pluripotent stem cell generation, Stem Cell. 28 (8) (2010) 1315–1325.
[32] M. Abad, et al., Reprogramming in vivo produces teratomas and iPS cells with totipotency features, Nature 502 (7471) (2013) 340–345.
[33] S. Hu, et al., NOTCH-YAP1/TEAD-DNMT1 Axis drives hepatocyte reprogramming into intrahepatic cholangiocarcinoma, Gastroenterology 163 (2) (2022) 449–465.
[34] A. Subramanian, et al., Gene set enrichment analysis: a knowledge-based approach for interpreting genome-wide expression profiles, Proc. Natl. Acad. Sci. U. S. A. 102 (43) (2005) 15545–15550.
[35] M. Kanehisa, et al., Data, information, knowledge and principle: back to metabolism in KEGG, Nucleic Acids Res. 42 (Database issue) (2014) D199–D205.
[36] F. Sampaziotis, et al., Cholangiocyte organoids can repair bile ducts after transplantation in the human liver, Science 371 (6531) (2021) 839–846.
[37] Y. Jin, et al., Stem cell-derived hepatocyte therapy using versatile biomimetic nanozyme incorporated nanofiber-reinforced decellularized extracellular matrix hydrogels for the treatment of acute liver failure, Bioact. Mater. 28 (2023) 112–131.
[38] K.M. Park, et al., Preparation of immunogen-reduced and biocompatible extracellular matrices from porcine liver, J. Biosci. Bioeng. 115 (2) (2013) 207–215.
[39] Y. Negishi, M. Nomizu, Laminin-derived peptides: applications in drug delivery systems for targeting, Pharmacol. Ther. 202 (2019) 91–97.
[40] B. Buchmann, P. Fernández, A.R. Bausch, The role of nonlinear mechanical properties of biomimetic hydrogels for organoid growth, Biophys Rev (Melville) 2 (2) (2021) 021401.
[41] L. Aloia, et al., Epigenetic remodelling licences adult cholangiocytes for organoid formation and liver regeneration, Nat. Cell Biol. 21 (11) (2019) 1321–1333.
[42] D. Serra, et al., Self-organization and symmetry breaking in intestinal organoid development, Nature 569 (7754) (2019) 66–72.
[43] W. Zhou, et al., Glucose and MMP-9 dual-responsive hydrogel with temperature sensitive self-adaptive shape and controlled drug release accelerates diabetic wound healing, Bioact. Mater. 17 (2022) 1–17.
[44] T. Vinikoor, et al., Injectable and biodegradable piezoelectric hydrogel for osteoarthritis treatment, Nat. Commun. 14 (1) (2023) 6257.
[45] S. Connolly, K. McGourty, D. Newport, The influence of cell elastic modulus on inertial positions in Poiseuille microflows, Biophys. J. 120 (5) (2021) 855–865.
[46] H. Wang, et al., Extracellular matrix-mimetic immunomodulatory hydrogel for accelerating wound healing, Adv Healthc Mater 12 (27) (2023) e2301264.

[47] K. Takahashi, S. Yamanaka, Induction of pluripotent stem cells from mouse embryonic and adult fibroblast cultures by defined factors, Cell 126 (4) (2006) 663–676.
[48] Z. An, et al., Sox2 and Klf4 as the functional core in pluripotency induction without exogenous Oct4, Cell Rep. 29 (7) (2019) 1986–2000.e8.
[49] F.X. Yu, et al., Regulation of the Hippo-YAP pathway by G-protein-coupled receptor signaling, Cell 150 (4) (2012) 780–791.
[50] I.M. Moya, G. Halder, Hippo-YAP/TAZ signalling in organ regeneration and regenerative medicine, Nat. Rev. Mol. Cell Biol. 20 (4) (2019) 211–226.
[51] G. Sorrentino, et al., Mechano-modulatory synthetic niches for liver organoid derivation, Nat. Commun. 11 (1) (2020) 3416.
[52] G. Halder, S. Dupont, S. Piccolo, Transduction of mechanical and cytoskeletal cues by YAP and TAZ, Nat. Rev. Mol. Cell Biol. 13 (9) (2012) 591–600.
[53] G. Pan, J.A. Thomson, Nanog and transcriptional networks in embryonic stem cell pluripotency, Cell Res. 17 (1) (2007) 42–49.
[54] M. Luo, et al., Rapid self-assembly mini-livers protect mice against severe hepatectomy-induced liver failure, Adv. Sci. 11 (21) (2024) e2309166.
[55] Y. Wang, et al., Reversal of liver failure using a bioartificial liver device implanted with clinical-grade human-induced hepatocytes, Cell Stem Cell 30 (5) (2023) 617–631.e8.
[56] Y. Liu, et al., Yap-Sox9 signaling determines hepatocyte plasticity and lineage-specific hepatocarcinogenesis, J. Hepatol. 76 (3) (2022) 652–664.
[57] K.P. Matchett, et al., Multimodal decoding of human liver regeneration, Nature 630 (8015) (2024) 158–165.
[58] J. Wang, et al., LINC00941 promotes pancreatic cancer malignancy by interacting with ANXA2 and suppressing NEDD4L-mediated degradation of ANXA2, Cell Death Dis. 13 (8) (2022) 718.
[59] Z. Gan, et al., Recent advances in defined hydrogels in organoid research, Bioact. Mater. 28 (2023) 386–401.
[60] L. Li, et al., Human apical-out nasal organoids reveal an essential role of matrix metalloproteinases in airway epithelial differentiation, Nat. Commun. 15 (1) (2024) 143.
[61] J. Willemse, et al., Hydrogels derived from decellularized liver tissue support the growth and differentiation of cholangiocyte organoids, Biomaterials 284 (2022) 121473.
[62] G.S. van Tienderen, et al., Extracellular matrix drives tumor organoids toward desmoplastic matrix deposition and mesenchymal transition, Acta Biomater. 158 (2023) 115–131.
[63] N. Gjorevski, et al., Tissue geometry drives deterministic organoid patterning, Science 375 (6576) (2022) eaaw9021.
[64] M. Qu, et al., Establishment of intestinal organoid cultures modeling injury-associated epithelial regeneration, Cell Res. 31 (3) (2021) 259–271.
[65] M.C. Heinz, et al., Liver colonization by colorectal cancer metastases requires YAP-controlled plasticity at the micrometastatic stage, Cancer Res. 82 (10) (2022) 1953–1968.
[66] D. Vanhoutte, et al., Thbs1 regulates skeletal muscle mass in a TGFβ-Smad2/3-ATF4-dependent manner, Cell Rep. 43 (5) (2024) 114149.
[67] J. Shen, et al., Hippo component YAP promotes focal adhesion and tumour aggressiveness via transcriptionally activating THBS1/FAK signalling in breast cancer, J. Exp. Clin. Cancer Res. 37 (1) (2018) 175.
[68] X. Zhao, et al., microRNA-222 attenuates mitochondrial dysfunction during transmissible gastroenteritis virus infection, Mol. Cell. Proteomics 18 (1) (2019) 51–64.
[69] S.M. Krishna, et al., High serum thrombospondin-1 concentration is associated with slower abdominal aortic aneurysm growth and deficiency of thrombospondin-1 promotes angiotensin II induced aortic aneurysm in mice, Clin. Sci. (Lond.) 131 (12) (2017) 1261–1281.
[70] T. Takebe, et al., Vascularized and functional human liver from an iPSC-derived organ bud transplant, Nature 499 (7459) (2013) 481–484.
[71] J. Guo, et al., A combined model of human iPSC-derived liver organoids and hepatocytes reveals ferroptosis in DGUOK mutant mtDNA depletion syndrome, Adv. Sci. 8 (10) (2021) 2004680.
[72] L. Warren, et al., Highly efficient reprogramming to pluripotency and directed differentiation of human cells with synthetic modified mRNA, Cell Stem Cell 7 (5) (2010) 618–630.
[73] M.J. Kratochvil, et al., Engineered materials for organoid systems, Nat. Rev. Mater. 4 (9) (2019) 606–622.
[74] S.J. Mun, et al., Generation of expandable human pluripotent stem cell-derived hepatocyte-like liver organoids, J. Hepatol. 71 (5) (2019) 970–985.
[75] J. Xu, et al., Generation of neural organoids for spinal-cord regeneration via the direct reprogramming of human astrocytes, Nat. Biomed. Eng. 7 (3) (2023) 253–269.
[76] I. Legnini, et al., Spatiotemporal, optogenetic control of gene expression in organoids, Nat. Methods 20 (10) (2023) 1544–1552.
[77] Y. You, et al., M1-like tumor-associated macrophages cascade a mesenchymal/stem-like phenotype of oral squamous cell carcinoma via the IL6/Stat3/THBS1 feedback loop, J. Exp. Clin. Cancer Res. 41 (1) (2022) 10.
[78] X.Y. Tang, et al., Human organoids in basic research and clinical applications, Signal Transduct Target Ther 7 (1) (2022) 168.
[79] S.P. Harrison, et al., Scalable production of tissue-like vascularized liver organoids from human PSCs, Exp. Mol. Med. 55 (9) (2023) 2005–2024.